Synthesis of Organic Nanofibers, for Non Linear Optical (NLO) applications

A Thesis

submitted to

Indian Institute of Science Education and Research Pune in partial fulfilment of the requirements for the BS-MS Dual Degree Programme

by

Naressh Kumar.R

Indian Institute of Science Education and Research Pune

Dr. Homi Bhabha Road,

Pashan, Pune 411008, INDIA.

April, 2020

Supervisor: Dr.R.Nagalakshmi

Naressh Kumar.R

Certificate

This is to certify that this dissertation entitled “Synthesis of Organic Nanofibers for Non Linear Optical (NLO) applications” towards the partial fulfilment of the BS-MS dual degree programme at the Indian Institute of Science Education and Research, Pune represents study/work carried out by Naressh Kumar.R at National Institute of Technology, Tiruchchirappalli, under the supervision of Dr.R.Nagalakshmi, Associate Professor, Department of Physics, during the academic year 2019-2020.

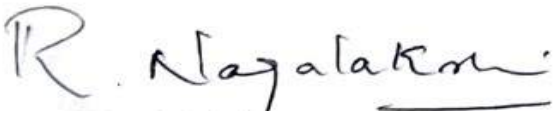

Dr.R.Nagalakshmi

10/4/2020

Committee:

Dr.R.Nagalakshmi

Dr.G.V.Pavan Kumar

Declaration

I hereby declare that the matter embodied in the report “Synthesis of Organic Nanofibers for Non Linear Optical (NLO) applications” are the results of the work carried out by me at the Department of Physics, Indian Institute of Science Education and Research, Pune, under the supervision of Dr.R.Nagalakshmi and the same has not been submitted elsewhere for any other degree

R Naresh Kumar

Naressh. Kumar.R

Date: 10/4/2020

Acknowledgements

First of all, I would like to thank my alma matter, Indian Institute of Science, Education and Research (IISER) Pune, and its Director, Mr. Jayant B. Udgaonkar, for giving me an opportunity to work on my 5th year Project outside my college. I would also like to thank National Institute of Technology (NIT) Tiruchchirappalli, and its Director, Mrs. Mini Shaji Thomas, for allowing me to continue my research work in NIT campus. I express deep thanks and gratitude for my Research Supervisor, Dr.R.Nagalakshmi,, for her guidance from the beginning, helping and aiding me through my research work. I would like to acknowledge Professor Dr.G.V.Pavan Kumar, for his assistance and evaluation. I also give thanks to St. Joseph College, Trichy, for SEM, FTIR and UV measurements, Mr. Nilesh Kulkarni of Tata Institute of Fundamental Research (TIFR) Hyderabad, for XRD measurements, and Professor Dr.T.C. Sabari Girisun of Bharathidasan University Trichy, for Z-scan measurements. I am very thankful to my lab mates and college mates, for assisting and helping my work. I am really appreciative of my family, friends and relatives, for supporting my work from the background. Finally, I thank the almighty, for keeping me in full health and giving good work environment thought my project.

Contents

List of Figures

List of Tables

Abstract

Lasers are one of the most important optical devices used in our society. This device has been implemented and is found in our day to day activities, and has many advantages, and limitations. Since lasers can be too powerful for an ordinary human to handle, there have been many studies and research work done since the advent of the device, to reduce the risk of using them, and to maximize its capabilities. Most phenomenon that gets directly affected due to the lasers can be categorized into Nonlinear optics. One of these phenomenon, is Nonlinear absorption, where absorption changes nonlinearly with respect to the incident laser beam. Some materials, increase or decrease its absorption nonlinearly, and these specific materials can be used to either amplify, or dampen the laser output for various uses. In my thesis, I try to analyse this property using Organic fibers, stating its efficiency in material preparation and its nonlinear absorption capabilities, compared to other organic/inorganic materials.

Part I

Introduction

Chapter 1

LASERs

LASERs, which can be abbreviated as 'Light Amplification by Stimulated Emission of Radiation', is recognized as one of the important optical devices produced in the past century. Albert Einstein initiated this revolution through his theoretical paper, which predicted stimulated emission in 1916. This led to scientists, developing MASERs, acronym for Microwave Amplifier by Stimulated Emission and Radiation, which in turn led to a primitive LASER device in 1960s, when MASERs was applied to light in visible region. In recent times, LASERs have significant importance and has reformed the Optic community as well as our society,used in various applications and with high research potential, becoming a part of our day to day life. Recent developments, include optical computing[1], laser treatments[2], etc.

1.1 Light-Matter interaction

Atoms consists of charged particles and it can be said that LASER emission is basically how these mentioned particles interact with the electromagnetic field. Assuming a simple case of hydrogen atom, having a single electron, which exhibits energy according to,

$$E_n = \frac{-13.6}{n^2} ev \qquad n = 1, 2, 3, ... \tag{1}$$

where 'n' specifies different states. The ground state corresponds to the lowest energy, whereas excited states correspond to electron in energy orbits away from nucleus. From (1), we can see that the energy is not quantized. Thus free electrons can come in contact with incoming photons of any frequency. In electromagnetic fields, the total energy in given electromagnetic field of frequency 'ν' is represented as,

$$E_n^{EM} = (1/2)h\nu + nh\nu \qquad n = 0,1,2,... \tag{2}$$

Here, 'n' represents total number of photons in the electromagnetic field. The energy of the radiation is quantized in units of hν, and the case of no photons in the field, aka, electromagnetic vacuum, still has total energy of 1/2hν.

If atoms and molecules are assumed to have discrete energy levels 'E_n' and 'E_m' interacting with electromagnetic field of frequency hν, such that, E_n - E_m = E_{n+1}^{EM}- E_n^{EM} = hν, then it can be said that the field is resonant with E_n to E_m transition of the atom or molecule. In the case of energy levels of the matter, having a nondiscrete, fine width 'ΔE' due to the interference from the environment, the frequency linewidth '$\Delta\nu$' resulting from the transitions of the energy levels is defined as,

$$\Delta\nu = \frac{\Delta E_n + \Delta E_m}{h} \tag{3}$$

The possibility of an atom or a molecule with energy levels 'E_m' and 'E_n' interacting with photon of defined frequency 'ν', is proportional to the lineshape function g(ν). This can be represented close to that of a symmetric function, with 'ν_o' as a frequency center, varying over the width '$\Delta\nu$' and peaks at $\nu = \nu_o$. The above function is normalized in such a way that,

$$\int_{all\nu} g(\nu)d\nu = 1 \tag{4}$$

The Theory of light-matter interaction from Einstein, explains thermal equilibrium between matter and light using three interaction processes. Consider a monochromatic EM field of Irradiance 'I', and frequency ν', proceeds to fall onto a bunch of atoms having energy levels 'E_1' and 'E_2' and corresponding number per unit volume of atoms in the energy levels (Population densities) as 'N_1' and 'N_2', so that $E_2 - E_1 \approx h\nu'$.The lineshape function g(ν) of 2-1 transition with respect to frequency ν' of incident light is also defined(see Fig 1.1).

Stimulated absorption is one of the three interaction processes through which, energy from a photon of frequency ν' is transferred from EM waves to the matter, whose atom can be lifted from initial state of energy 'E_1' to final state of energy 'E_2'. The rate of occurrence of stimulated absorption per unit volume,'$R_{St.Abs}$' , can be written as,

$$R_{St.Abs} = B_{12}g(\nu')(I/c)N_1 \tag{5}$$

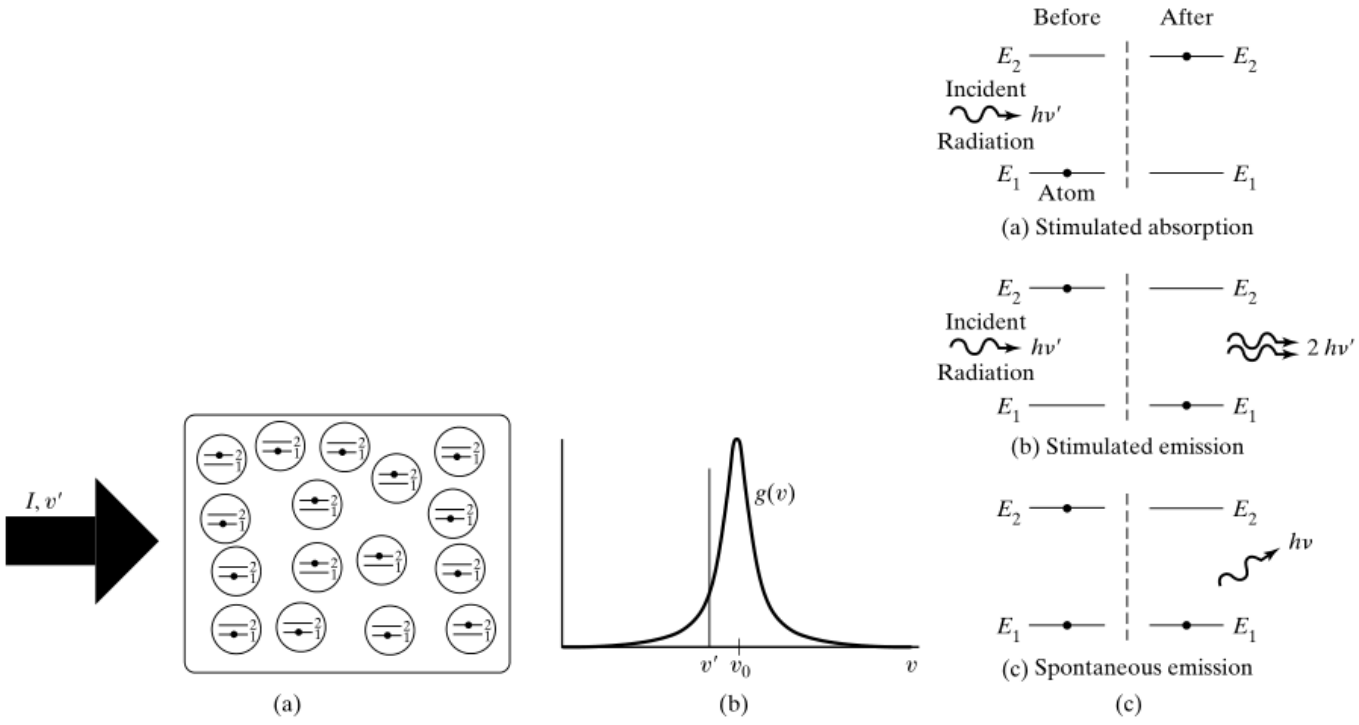

Figure 1.1: Figures involving (a) Experimental setup, (b) Lineshape Function $g(\nu')$ defined above, (c) Three different processes of light matter interaction(Adopted from [3]).

When a photon of frequency ν', stimulates an atom in excited state 'E_2' to jump to lower state 'E_1', this process is known as stimulated emission. This emission results in the atom releasing a photon of same energy, phase, direction, and polarization as that of incident photon, hence twin photon emission. The rate per unit volume of stimulated emission, $R_{St.Em}$, is

$$R_{St.Em} = B_{21} g(\nu')(I/c) N_2 \tag{6}$$

If a photon of frequency ν' is spontaneously emitted from an atom in an exited state, without any photon interaction on the specified atom, this is known as spontaneous emission. This process can also be explained as atoms interacting with electromagnetic vacuum. The emission rate per unit volume for the process is,

$$R_{Sp.Em} = A_{21} N_2 \tag{7}$$

The parameters 'B_{12}', 'B_{21}'. and 'A_{21}' are the Einstein A and B coefficients for corresponding stimulated absorption, emission and spontaneous emission. For the thermal equilibrium to exist in the above mentioned scenario, the following equations are necessary,

$$\frac{A_{21}}{B_{21}} = 8\pi h\nu^3/c^3 \tag{8}$$

$$B_{12} = B_{21} \tag{9}$$

These equations explain the relations between the Einstein coefficients. From (5) and (6) along with (9), one can conclude, the ratio of rate of stimulated emission to that of absorption equals to the ratio of corresponding population densities of upper and lower energy levels. Since population densities are directly proportional to the probability that a specified atom will be in that particular level, using Boltzmann distribution,

$$\frac{P_2}{P_1} = \frac{N_2}{N_1} = e^{-(E_2-E_1)/k_bT} < 1 \tag{10}$$

In thermal equilibrium, we can conclude from the above equation that stimulated absorption is found more than the process of stimulated emission. So, in order to amplify incident field, energy must be pumped to the material so that the atoms, come out of the equilibrium and populate the upper levels. This phenomenon is known as population inversion and plays a major role in laser emission.

1.2 Properties of lasers

A Given LASER primarily consists of

- Pump, which acts as external energy source. This creates the population inversion that amplifies the output from the Laser medium.
- Gain Medium, which contains the media with quantized energy levels. This decides the wavelength of the LASER. It can also involve other levels during the process, other than the two defined energy states, which might be due to the mixture of materials to form a gain media. One of the examples of multi-media laser is Nd:YAG laser, introduced in 1964[4].
- Resonator, using optical feedback to move photons back and forth through the media. It is designed with an optical cavity, providing directionality.
- Cooling system, which improves the efficiency of the device by cooling the laser medium. This reduces the thermal/heat energy produced by the laser, which can damage other components.

The laser source is focusable, spatially and temporally coherent, due to the unique properties of the stimulated emission process. The above factors also result in high irradiance of the laser. It is highly monochromatic and can be specified within a certain frequency linewidth. This linewidth, comes from the random spontaneous emissions, which occur in the media other than the specified stimulated emissions. If required, the laser can be pulsed, giving out bursts of radiation with durations around femtoseconds. Due to the above properties of irradiance and pulsed beams, shining lasers upon materials and media, lead to unique properties and deviations from the known phenomena, leading to Nonlinear Optics.

Chapter 2

Non Linear Optics

One of the properties of a given material, is how under an applied electric field, the molecules get displaced, inducing dipole moment per unit volume (polarization). Polarization density can be defined as $P = Np$, where 'N' is number density of dipole moments, 'p' is individual dipole moment and 'E' represents applied Electric field. When linear dependence between 'E' and 'p' vanishes due to high value of electric field, or 'N' varies non linearly in the optical field (due to optical field being a laser medium where total number of atoms staying in the energy levels, depend on intensity of light), we enter the non linear regime. Expanding the above proportionality using Taylor series around $E = 0$ and replacing different order derivatives of 'P' with respect to 'E' with nonlinear coefficients(see [5]), we get the equation as,

$$P = \varepsilon\chi E + 2dE^2 + 4\chi^{(3)}E^3 + ... \tag{11}$$

where 'd' and '$\chi^{(3)}$' are second order and third order non-linear coefficients. If the medium is centrosymmetric, P-E function will have odd symmetry, thus 'd' vanishes and the lowest order of nonlinearity possible, is that of third order.

Consider a generic case for a material with/without loss, but has dispersion. Defining $\tilde{E}_n(r,t)$ as sum of positive and negative frequencies of Electric Field vector of the high intensity wave, we can represent it as,

$$\tilde{E}_n = \tilde{E}_n^{(+)} + \tilde{E}_n^{(-)} \tag{12}$$

where $\tilde{E}_n^{(+)} = E_n e^{(-i\omega t)}$, and $\tilde{E}_n^{(-)} = \tilde{E}_n^{(+)*} = E_n^* e^{(i\omega t)}$

The last equation makes sure that the value of Electric field vector would be real, as it has to be a physical field. By rewriting $E_n = E(\omega_n)$ and considering slowly varying field amplitude $E(\omega_n) = A(\omega_n)e^{ik_n.r}$, The

reality condition, implies $E(-\omega_n) = E(\omega_n)^*$ and $A(-\omega_n) = A(\omega_n)^*$.

Therefore The total field and nonlinear polarisation vectors can be written in similar way,

$$\tilde{E}(r,t) = \sum_n E(\omega_n) e^{-i(\omega_n)t} = \sum_n A(\omega_n) e^{i[k_n r - (\omega_n)t]}$$
$$\tilde{P}(r,t) = \sum_n P(\omega_n) e^{-i(\omega_n)t} \tag{13}$$

Components of second order susceptibility tensor $\chi^{(2)}_{ijk}(\omega_n + \omega_m, \omega_n, \omega_m)$ can be considered as proportionality constant relating the amplitude of nonlinear polarisation to that of the product of field amplitudes. Hence, the above equation, can be changed as,

$$P_i(\omega_n + \omega_m) = \sum_{jk} \sum_{(nm)} \chi^{(2)}_{ijk}(\omega_n + \omega_m, \omega_n, \omega_m) E_j(\omega_n) E_k(\omega_m) \tag{14}$$

2.1 Second Harmonic Gerenation

Given electric field of frequency 'ω' with complex amplitude '$A(\omega)$', The Field can be expanded as,

$$E(t) = Re[A(\omega)e^{(i\omega t)}] = 1/2[A(\omega)e^{(i\omega t)} + A^*(\omega)e^{(-i\omega t)}] \tag{15}$$

Putting Eq (15) onto the second part of the Eq (11) representing for second order non-linear case, we get,

$$P^{(2)}(t) = P^{(2)}(0) + Re[P^{(2)}(2\omega)e^{(2i\omega t)}], \qquad where \tag{16}$$

$$P^{(2)}(0) = dA(\omega)A^*(\omega) \tag{17}$$

$$P^{(2)}(2\omega) = dA^2(\omega) \tag{18}$$

The optical field which was scattered, has a component at second harmonic of the incident electric field and another component corresponding to a steady polarization density(Optical rectification).

Lets go back to the general case defined by equation (14) with input frequencies 'ω_1' , 'ω_2' and frequency sum $\omega_3 = \omega_1 + \omega_2$. Summations over '$\omega_1$' and '$\omega_2$' in the vector equation implies,

$$P_i(\omega_3) = \sum_{jk} [\chi^{(2)}_{ijk}(\omega_3, \omega_1, \omega_2) E_j(\omega_1) E_k(\omega_2) + \chi^{(2)}_{ijk}(\omega_3, \omega_2, \omega_1) E_j(\omega_2) E_k(\omega_1)] \tag{19}$$

Using Intrinsic permutation symmetry, and assuming there is only one input frequency 'ω_1' and generated frequency, $\omega_2 = 2(\omega_1)$, then one can change the equation as,

$$P_i(\omega_2) = \sum_{jk} \chi^{(2)}_{ijk}(\omega_2, \omega_1, \omega_1) E_j(\omega_1) E_k(\omega_1) \tag{20}$$

The Eq (20) refers the degenerate case of SHG. We can also see that the factor of 2 will arise from $\sum_{nm}$ in Eq (14), as keeping n + m fixed while changing 'n' and 'm' adds degeneracy factor in the final equation. Therefore, in general,

$$P_i(\omega_n + \omega_m) = D \sum_{jk} \chi^{(2)}_{ijk}(\omega_n + \omega_m, \omega_n, \omega_m) E_j(\omega_n) E_k(\omega_m) \tag{21}$$

where 'D' represents total number of distinct permutations of applied field frequencies 'ω_n' and 'ω_m'. When $D = 2$, it is the case of sum-frequency generation, where both values of frequency are different. By changing one of the signs of the frequency in the previous equation, it can result in frequency downconversion. One can simplify the susceptibility tensors even more using symmetries (Refer [6]).

Within a very small angle around a precise direction, if all the microscopic dipoles emit coherantly due to the incident optical field, the field radiated by the dipoles are all in phase. This is referred to as phase matching. Using conservation laws in previous equations, one can get phase matching conditions with respect to wavenumbers in mathematical terms,$k_{\omega_m} + k_{\omega_n} = k_{\omega_m + \omega_n}$. In degenerate case of SHG, we can simplify with incoming wave with wavenumber' k_1',output wave with wavenumber' k_3' as,

$$2k_1 = k_3 \tag{22}$$

2.2 SHG as Three wave Mixing

Considering field '$\mathscr{E}(t)$' as superposition of three waves with angular frequencies, 'ω_1', 'ω_2', 'ω_3', with complex amplitudes, 'E_1', 'E_2' and 'E_3'. Using the same equational method as (15),we can write it as a summation,

$$\mathscr{E}(t) = \sum_{q=\pm1,\pm2,\pm3} (1/2) E_q e^{(i\omega_q t)} \tag{23}$$

where $\omega_{-q} = -\omega_q$ *and* $E_{-q} = -E_q^*$. Substituting (23) in second part of (11), and using the resulting Polarization Density in basic wave equation in nonlinear medium with radiation source $\mathscr{S} = -\mu_o \frac{\delta^2 P_{2NL}}{\delta t^2}$, the

result is in form of Helmholtz equations,

$$(\Delta^2 + k_j^2)E_j = -S_j \tag{24}$$

where' S_j' is amplitude of component of '$\mathscr{S}$' with frequency 'ω_q' and $k_q = n\omega_q/c_o$.

Since SHG, is a degenerate case, where $\omega_1 = \omega_2 = \omega,\ \omega_3 = 2\omega$, we get SHG Coupled Equations as,

$$(\Delta^2 + k_1^2)E_1 = -2\mu_o\omega_1^2 dE_3E_1^*$$

$$(\Delta^2 + k_3^2)E_3 = -\mu_o\omega_3^2 dE_1E_1 \tag{25}$$

Assuming the waves are collinear, propagating in z direction with perfect phase matching, one can derive photon flux densities '$\phi(z)$', by applying slowly varying envelope approximation, to coupled equations (25)(Refer [7]). Thus, by simplifying $g^2 = 4\hbar d^2\eta^3\omega_1^3,\ \gamma = \sqrt{2}ga_1(0)$, we conclude,

$$\phi_1(z) = \phi_1(0)sech^2\frac{\gamma z}{2}$$

$$\phi_3(z) = \frac{1}{2}\phi_1(0)tanh^2\frac{\gamma z}{2} \tag{26}$$

where $\eta = \eta_0/n$ is the impedance of the medium,' η_0 ' is the impedance of free space, $a_1(0)$ defines amplitude of fundamental wave at the input to the device(z = 0), nonlinear parameter 'd', and refractive index 'n'.

2.3 Efficiency of SHG

Efficiency of SHG for a nonlinear material with interaction region of length 'L' can be described as ratio of wave intensities of second harmonic wave at length 'L' to that of fundamental wave at the input to the device. Hence $\eta_{SHG} = \frac{\hbar\omega_3\phi_3(L)}{\hbar\omega_1\phi_1(0)} = tanh^2(\gamma L/2)$.

In the case of large input intensity, or large second order nonlinear parameter, or long cel(larger value of L), it implies γL is large and the efficiency is close to 1. If γL is small, $tanhx \approx x$. Thus,

$$\eta_{SHG} \approx (1/4)\gamma^2L^2 = 2d^2\frac{\eta_0^3}{n^3}\omega_1^2L^2\frac{P}{A} \tag{27}$$

where 'P' is incident optical power at fundamental frequency and 'A' is the area of cross section.

To maximise efficiency, one can use pulsed lasers, where the energy is restrained to get bursts of large power peaks. We can also provide larger interaction lengths(L), and can focus the beam to a small cross sectional area. In thick crystal (Fig 2.1), assuming input laser of gaussian beam, focused on beam width W_o, maintaining cross sectional area $A = \pi W_o^2$ over a depth of $L = 2z_o = 2\pi W_o^2/\lambda$, the ratio of $L^2/A = A/\lambda$. Therefore, in this case, beam must be focused to a larger spot size, with respect to its large depth of focus.

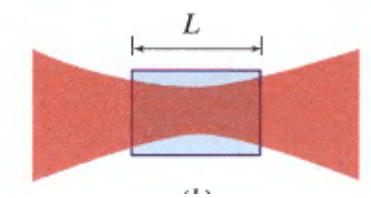

Figure 2.1: Laser Focusing in Thick Crystal

2.4 Third-Order Nonlinear Optics

In Eq (11), The third term $P_{3NL} = 4\chi^{(3)}E^3$, represents third order nonlinearity. As stated above, in centrosymmetric media, Second order term vanishes due to odd symmetry, and the primary nonlinear applications come from third order. This media is called Kerr media.
Substituting (15) to 'P_{3NL}' described above, The results contain components at frequency ω *and* 3ω,

$$P_{NL}(\omega) = 3\chi^{(3)}|E(\omega)|^2E(\omega) \tag{28}$$

$$P_{NL}(3\omega) = 3\chi^{(3)}E^3(\omega) \tag{29}$$

The component of frequency '3ω', implies third harmonics is generated. This process of Third Harmonic Generation can also be interpreted as Second Harmonic Generation, followed by sum-frequency generation of fundamental and second harmonic waves. The other component leads to nonlinear contribution to refractive index by the wave of frequency'ω'. Therefore, the total refractive index experienced for given intensity of light 'I' in this case can be written as,

$$n = n_o + n_2 I \tag{30}$$

To calculate 'n_2', we start with incremental change in susceptibility occured during the process, given by $\varepsilon_o \Delta\chi = \frac{P_{NL}(\omega)}{E(\omega)} = 6\chi^{(3)}\eta I$. Differentiating relationship between refractive index and susceptibility, we get,

$$\Delta n = \frac{3\eta}{\varepsilon_0 n}\chi^{(3)} I = n_2 I \tag{31}$$

This effect is known as optical Kerr effect, where 'Δn' is proportional to the square of the Electric Field. This is one of the applications of nonlinear refraction.

2.5 Nonlinear Absorption and Refraction

When a given sample experience light of weak irradiance, the input and output fluence increases linearly with respect to increase in irradiance of the input light. This is a simple representation of Beer's Law, where transmittance remains almost constant. The attenuation of this beam, when it is propagating along the medium of the sample along z direction can be described as $\frac{dI}{dz} = -\alpha I$, where 'I' is beam intensity, and 'α' is absorption coefficient of the given medium. This leads to Beer-Lambert law $I(z) = I(0)e^{(-\alpha z)}$.But, once light crosses the threshold value of irradiance of a particular material, the output fluence varies differently after increasing the input fluence of the light. If the given sample exhibits nonlinear behaviour, then the it could either exhibit Saturable Absorption(SA), or Reverse Saturation Absorption(RSA) effects. In this case, the differential equation has to be changed according to the nonlinear application,

$$\frac{dI}{dz} = -\alpha I - \beta I^2 - \gamma I^3 - ... \tag{32}$$

where' β' represents two photon absorption coefficient, 'γ' represents three photon coefficient, and etc. These high intensity laser beam interactions, can lead to changes in real and imaginary parts of polarization. This imaginary part exhibits the n-photon resonance, when two levels of atoms/molecules of the given nonlinear sample can be connected with n optical quantum levels of the system, therefore associated with multiphoton resonance.

We have already got a glimpse of nonlinear refraction with optical kerr effect in Eq (30). Other unique phenomena caused by the nonlinear refractive index(NRI), include Self Focusing/Defocusing(when intense laser beam passes through thin nonlinear material, the NRI change in such a way that, the resultant index, copies the intensity pattern of the transverse wave),Spatial Solitons (when highly intense beam passes through thick nonlinear material, the NRI change nonuniformly in such a way that, the material acts as a graded-index waveguide), Self Phase Modulation(Phase shift occuring due to the incoming optical beam in a nonlinear material with defined NRI), Electronic Polarization, and can even change the physical properties of the media, like concentration and temperature.

Chapter 3

Organic Nanofibers

When static charge is given to a molecule, as stated before, dipole moment gets induces, due to charge displacement. Expanding polarization of the molecule using power series, we get $p = p_o + \alpha E + \beta EE + \gamma EEE + ...$, where, '$p_o$' is ground state polarization and 'α','β', and 'γ', are linear, quadratic, and cubic polarizabilities. Hyperpolarizabilities usually changes according to photon energy of applied electric field, oscillator strength of the transition in the given molecule and change in dipole moment during the transition process.

Due to the delocalized π electrons and corresponding conjugations in organic materials, interaction with high intense optical fields such as LASERS, can result in electron distribution being perturbed. This will result in redistribution of atoms and molecules in the materials, and can lead to modification of induced dipole moment and hyperpolarizabilities of the material. This will, in turn, affects the nonlinear optical effects of the material[8].

Organic molecules can be either produced as single crystals, or can be fabricated into waveguides, in order to display most of the NLO applications. It is easy to analyze that both single crystals and optical waveguides produced, must be defect free, compatible, polishable, and must have optimal orientation to have very less scattering losses/degradation of the output laser beam.

One dimensional and aligned nanostructures as nanofibers, are highly researched and studied upon by the nano industry, mainly due to its different applications in electronic and optical properties. It has a possibility to show properties, with varying deviations with respect to their nonaligned counterparts. These nanofibers have the potential to be smoothly implemented in/as a device due to its ease in usage, preparation and micromanagement.

Chapter 4

Aim of the Thesis

In my research work, I am trying to obtain organic molecules which exhibit high nonlinear optical properties, as one dimensional single crystal. I am implementing my idea in the form of nanofibers, where the organic molecules are embedded inside the polymer matrix. The fibers are produced using electrospinning technique, and is studied for nonlinear absorption of the third- order, using z-scan technique. I have chosen Urea as my organic material, and PVA as the polymer matrix in which the organic molecule is embedded on.

Charge-transfer molecules such as 2-methyl-4-nitroaniline(mNA) or urea, exhibits an increase in second order and third nonlinear response in nanofibers than that of the corresponding single crystal bulk[9,10]. It is being hypothesized that the crystalline size of these molecules is less than coherence length of the Harmonic Generation in the nanofibers. Therefore, if the incident laser's propagation distance inside the nanofiber, is less than that of the coherence length, then all the dipole's response add up in phase and exhibit better nonlinear properties. Since we create fibers using electrospinning, where the resulting diameter can be in the range of nanometers, which is less than the general coherence length of Harmonic Generation for the specified organic molecules, the response of each dipole is phase matched[11,12].

Crystalline urea can be phase matched to 238nm and has high optical damage threshold. Coupled along with a high nonlinear coefficient values, Urea is one of the most versatile nonlinear organic materials available. One of the shortcomings that comes along with urea is that, the crystalline growth of Urea is hard to manipulate and is slow. This is negated in my research work, as it is easy to prepare nanofibers using electrospinning once the parameters are confirmed, and is expected to form 1-D single crystal inside the fiber. Since the polymer, does not show any nonlinear deviation, any characteristics of nonlinear optical properties, comes from that of the organic molecule, which is urea in my case.

Part II

Material Preparation and Methods

Chapter 5

Electrospinning

Electrospinning process involves applying very high electric field into the solution, inorder to obtain fiber jets. When the solution contains organic molecules exhibiting large dipole moment along with the polymer solution, as the nanofibers form, due to the Shear stress and Coloumbic forces acting on the polymer solution, the electrostatic molecular arrangement will also affect the molecule along with the polymer. Therefore there is a possibility of creating nanofibers with anisotropic polar properties, where the organic molecules reside inside the polymer matrix[13]. The mixture can also result in an inclusion complex, as these results depend on the material characteristics of the individual media[14]. Now, if this process in run long enough to form a thick fiber array, we can fabricate a single crystal-like pattern that resembles a bulk.

5.1 Theory

Electrospinning is a technique, through which, one-dimentional nanofibers can be produced from solutions of organic nature. Initially, A Highly Viscous Organic solutions of either simple molecule, or a mixture of required ratio, is prepared and loaded in the syringe. The syringe tip is flattened and its needle is connected to a very high voltage source. It is then locked tightly within a piston pump. The Collector Plate is prepared for Y-axis Electrospinning, and Collector Drum is kept ready for X-axis Electrospinning. Once the parameters are verified and checked, we start to increase the voltage. As we increase, the free charges induced in the solution, move towards the collector/drum with opposite polarity and the droplet at the tip gets stretched. This process results in formation of Taylor cone.

At the critical point, i.e., when electrostatic energy caused by the voltage is more than the surface tension of the organic solution, the tip of Taylor cone inverts and a stream/jet of liquid bursts out of syringe, and

moves towards the collector/drum. If the cohesion between molecules are high enough, then the stream/jet ejected from the syringe do not break up and produces a continuous fiber jet, otherwise the solution gets electrosprayed. As the charges move towards the surface of the fiber, the jet undergoes a whipping process, where due to electrostatic repulsion at the small bends at the fiber, gets elongated and thinned out(Fig 5.1). The solvent evaporates at the collector's end, as the process continues and the dry fibers in the size of nanometers get clustered/arrayed in the collector/drum(see [15] for detailed explanation).

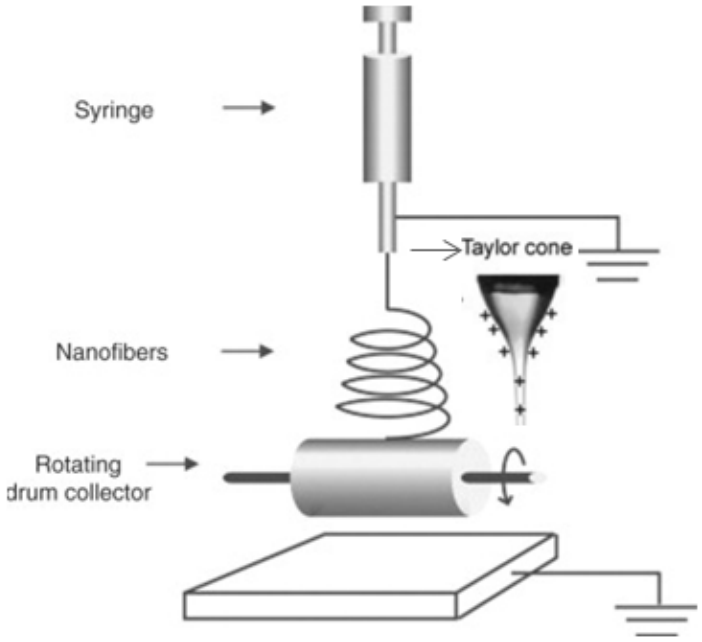

Figure 5.1: Electrospinning process adopted from [16]

5.2 Different Parameters and its effects

The process of electrospinning, even though is easy to setup and operate, it is one of the complex experiments. This is due to the fact that, once the process of electrospinning begins, there are a lot of Parameters and Factors that are in full play.

- One of the Basic Parameters include the external Voltage, applied to the syringe. If our fixed voltage is more than the threshold of the sample, it can result to changes in shape of the jet initiating surface, making it unstable, and can lead to different structures and shapes of the fibers, rather being streamlined. A steep increase in voltage during the process can result in beaded morphologies. This could

affect the efficiency and transmittivity of the layer formed, as it reduces the surface area.

- Flow rate can also be considered as a basic parameter, This stems from the fact that the initially fixed flow rate controls the jet velocity and material transfer rate to the collector/drum. Less flow rate prohibits formation of fibers, because the rate is not enough for the formation of Taylor cone. High flow rate causes beaded structures, and even higher flow rate can lead to spraying, as there is no time for formation of the cone.

- Molecular weight/Weight or Volume ratios of the solution will definitely affect the process, as, lower than optimal concentration can result in electrospraying (due to low surface tension) and higher than optimal concentration can constrain the formation of nanofibers (due to high viscosity, blocking the tip of the syringe).

- Since the electrode of opposing polarity is found at this end, its spatial position with respect to the syringe matters. Too far away from the syringe can lead to no formation of fibers as it can't influence the charges from the jet and too close might result in wet fibers because there is no time for the solvent to evaporate.

- Environment Factors including enclosed air and gas(sometimes including vacuum conditions), temperature and relative humidity of the enclosed setup, can affect the process as the high voltage applied during the process can create an electric discharge(breakdown voltage) in the surrounding gas, which can control the charge retaining capacity of the fibers.

5.3 Advantages and limitations

Advantages of this process, include

- The Setup is easy to work with, and requires less effort as most of the process are mechanised.

- The Parameters can be loaded into the program and will be kept constant throughout the process.

- If all the parameters required are good, then the electrospinning process can produce fibers to the range of 200 nanometers.

- The process can be versatile, as one can add gas to the setup chamber, that will act as the environment for the process.

Limitations of electrospinning, come from

- The Setup, which might require high maintenance, as there are mechanised moving parts, and involves high voltage.
- It can take days, even weeks, to obtain the right viscous solution of a mixture and to find the optimal parameters for the improvised solution.
- The syringe tip,if not flattened properly, can lead to distorted Taylor cone during the process and can result in fibers of uneven diameters.
- Not tightly fixing the syringe on the pump, can make it wobble, resulting in uneven spreading of the fiber along the layer bed.
- This process can be used for creating nanofibers of organic materials/solutions, only. This is not suitable for any other media(includes inorganic materials).

Chapter 6

Material Preparation

In my research work, I have tried to create Polyvinyl Alcohol(PVA)-Urea nanofibers, with three varying concentration ratios, and tried to find how the structure and its nonlinear applications change with respect to each other, compared to that of the crystal urea in bulk. Initially, 0.2 g of PVA is added to at least 6ml warm water(common solvent), and is heated to $105 - 115^{o}$C. It completely dissolves around 3hrs, forming a thick and transparent viscous liquid. Stop the process if the volume is less than 1.5 ml, and add normal water upto 1.5ml after cooldown time of 3hrs, otherwise boil the solution until the volume drops to 1.5ml and enter the cooldown time.

After cooling, I added 0.1g of Urea into the solution under constant stirring, and is stirred for an hour, before loading it in syringe for the process of electrospinning. Similarly, two batches of solution was prepared, with 0.15g and 0.2g of Urea added to the PVA Solution and stirred before electrospinning. The X-axis Electrospinning was done using E-Spin Nanotech electrospinning unit, with voltage range 0-30kV, and the parameters are loaded to the inbuilt bunifu software.

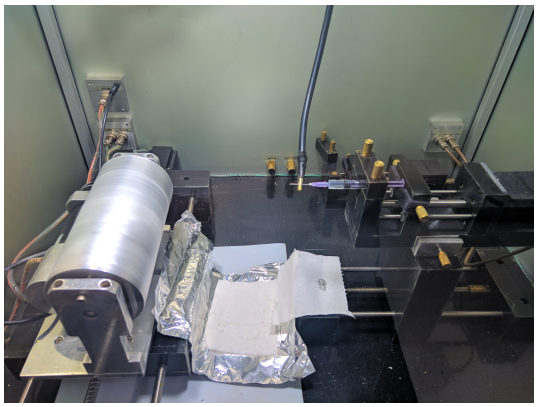

Figure 6.1: Electrospinning in motion

The Voltage applied on the syringe needle is 19 kV, with Flow rate, around 0.2ml/hr. The distance between the syringe tip and the drum is 17cms, with syringe of the needle measured to be 8.92mm and the drum, set to rotate at 800rpm. Every other parameters is constant and kept same with respect to the normal room environment (Fig 6.1). Repeated coatings is done on the sample, if concentration of the layer bed is not enough.

Three batches of samples with PVA-Urea weight ratios 2:1, 4:3, and 1:1, is collected (Fig 6.2), studied for structural alignment and properties, and is tested for nonlinear absorption using open z-scan measurements.

Figure 6.2: Resultant PVA-Urea Fibers, with the centre peeled for z-scan measurements.

Chapter 7

Characterization Techniques

7.1 Scanning Electron Microscopy

Scanning Electron Microscope can be considered as the modified and enhanced version of an electron microscope, in which, an electron probe with narrow electron beam is incident on the surface of the material, to give three dimensional image of the sample with characteristic depth of field. This characterization technique, can be used to study structure of the sample in place, including surface microappearances, microstructural phases and features in crystals, and finding crystal molecule's orientation, by studying orientation of individual grains of the material in place.

Theory and Instrumentation

When an electron probe with a narrow electron beam, is made to fall upon the surface of the sample material, it produces either secondary electrons or backscattered electrons.

Some electrons of the incident beam, can pass through the sample, with lower kinetic energy on the other end. This is due to the electrons, passing on some of its energies to the neighbouring surface of the atoms in the sample material, ionising them. These 'Secondary electrons', diverts from its initial path, and is collected by positively charged detector in the other end, to study topographical information. Some other electrons can bounce back or gets reflected back as a result of collision with respect to the atoms of the sample. These 'Backscattered' electrons, deflect corresponding to the atomic number of the collision atom, and these electrons are collected and studied to find about different parts of the material with different atomic numbers (Refer [17] for more explanation).

In the setup shown below (Fig 7.1), The Electron discharge is produced by the electron gun placed at top, and the beam is formed using various lens placed on the sides. The condenser lens reduces crossover diameter, whereas, the objective/probe forming lens focus the electrons as a narrow beam. Then, the beam is made to sequentially cross across in rectangular segments of the material, using Raster scanning. The emitted electrons are collected, and is amplified and studied along with the corresponding picture points on CRT screen.

The SEM in my research work was analysed using Zeiss EVO-18, with secondary e-image resolution of 50 nm and magnification upto 50-100 K (Depending on the sample).

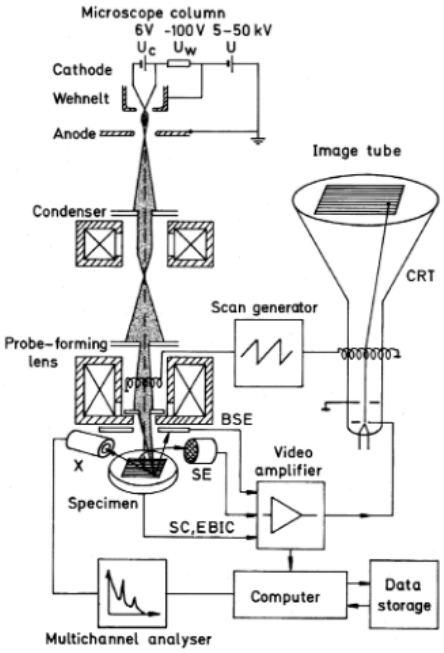

Figure 7.1: Schematic diagram of SEM(Adopted from [18])

7.2 X-Ray Diffraction

X-ray Diffraction(XRD), is one of the powerful and analytical characterization techniques, used for calculating preferred phase of the material in place. This technique can be used to find average crystal size, its unit cell measurements, and to determine sample purity. Initially introduced by Max von Laue[19], This technique depends on X-rays being produced and when it is accelerated onto the target material, electrons are ejected and the subsequent spectra is studied in detail for phase identification.

Theory and Instrumentation

When X-ray beam is targeted onto a crystalline solid at varying incident angles, it will be diffracted according to the crystallographic planes of the material. Under certain conditions, the output X-ray spectra undergoes constructive interferences, creating a stronger output intensity.

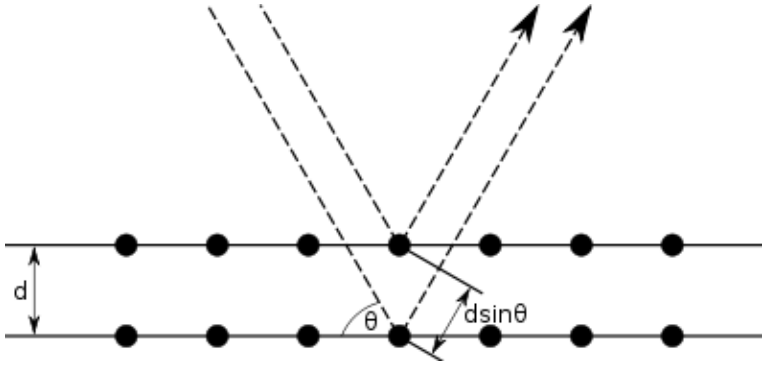

Figure 7.2: Bragg's Law(Courtesy of Wikipedia)

This condition is given by Bragg's Law, which states that, under a certain input angle θ, the constructive interference occurs if and only if, $n\lambda = 2dsin\theta$, where 'n' is an integer, 'd' is distance between crystallographic planes or 'd_{hkl}', and 'λ', represents wavelength of the incident X-ray. This can be easily proved by measuring path difference of the case where in-phase incident waves fall onto the crystal, giving in-phase diffracted rays (Fig 7.2). By varying the incident angle in values of '2θ', We can get XRD Pattern of 2θ vs Intensity of the emitted wave, to study its structure. We can also find the crystalline size of the material, using Scherrer formula $D = \frac{0.9\lambda}{wcos\theta}$, where 'w' is the Full Width at Half Maxima (FWHM) of the XRD peak in measure (Refer [20]).

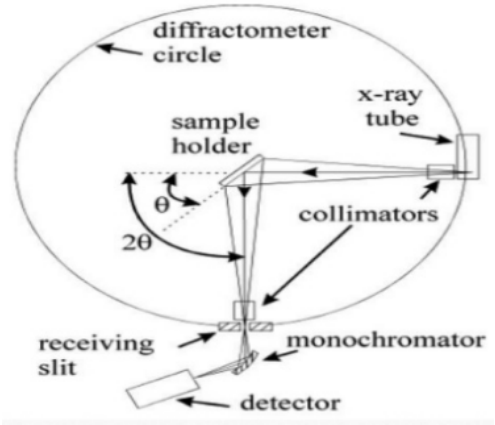

Figure 7.3: Simple X-Ray Diffractometer

Typical X-ray diffractors (Fig 7.3) consist of X-ray tube(Cathode ray tube), heating up a filament to produce X-rays, which fall on the material placed in holder, the diffracted rays are measured using detectors. In my research work, The XRD Pattern was measured using Panalytical X'pert PRO X-Ray Diffractometer, with wavelength of incident Cu-Kα radiation around 0.15406 nm, and was measured in ambient temperature and pressure.

7.3 Fourier-Transform Infrared Spectroscopy

Fourier-Transform Infrared (FTIR) Spectroscopy, is a characterization technique, used for studying molecular composition, and structure of the sample in place by identifying the presence of certain functional groups in the molecule. This technique, which was initially discovered to study stars[21], involes the study of infrared spectra, emitted by the material upon shining polychromatic light. This method can be used to identify unknown materials in the sample, sample's quality or consistency of the sample.

Theory and Instrumentation

In this spectroscopy, the sample is irradiated with polychromatic light. When the energy of the incoming light matches the energy required for the particular bond in the sample to vibrate, a photon from the incident light is absorbed . For the vibration to exhibit infrared emission, there must be a change in dipole moment of the material during the process. By comparing Transmittance percent to the Energy of the light, which is converted with respect to wavenumber, one can get the vibrational frequencies of the molecules. This is because, wherever there is a peak in the spectral plot, that implies some of the energy was absorbed due to the resonance caused by some molecule in the material. The peaks intensity, depend on how much there is change in dipole moment, for that particular molecule.

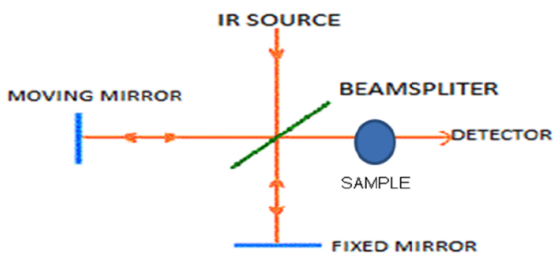

Figure 7.4: Schematic Diagram of FTIR Spectrometer

.

FTIR Spectrometers (Fig 7.4) consist of radiation source, which produces polychromatic light. This falls on the sample, through interferometer. The remaining energy measured by the detector, is amplified, converted to digital and is Fourier transformed to get the spectral plot. For this research work, the sample was measured, using, Perkin Elmer Spectrum Two FTIR/FIR spectrometer in the range of 4000-400 cm^{-1}, due to organic compounds exhibiting photon absorption in this region.

7.4 Ultra-Violet Visible Spectroscopy

Ultra-Violet Visible (UV–Vis) spectroscopy, is the characterization technique, where linear absorption/reflective spectroscopy is measured with respect to UV and visible light.For this region of EM spectrum, molecules in the sample, experience electron transitions. While Fluorescence spectroscopy attempt to study transitions from the excited to ground state, this technique studies transition from ground state to excited state.This technique can be used to find molecular compounds that can absorb UV and can also be used to find impurities in organic molecules.

Theory and Instrumentation

When the sample has molecules with bonding and non-bonding electrons, if it is incident with UV and Visible light, it can be excited to higher anti-bonding molecular orbitals. Lower the energy gap between the Highest Occupied and Lowest Unoccupied Molecular Orbitals, it is easier to excite the electrons and longer the wavelength of absorbed light (See Fig 7.5 for transitions and conditions).

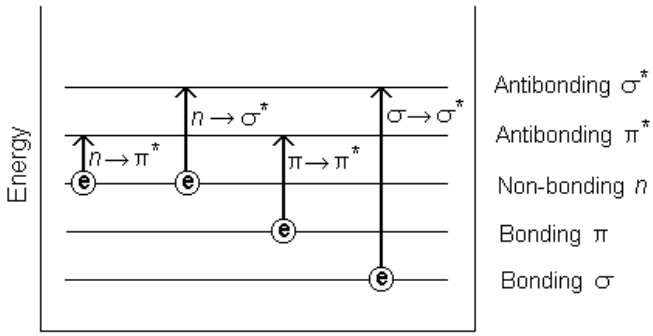

Figure 7.5: Electron transitions in organic molecules (Possible transitions in order σ–$\sigma^* > n - \sigma^* > \pi$–$\pi^* > n$–$\pi^*$.)

.

Therefore, when molecules in the material are incident to light, having energy matching that of transition of electron, that energy gets absorbed and that electron promotes to higher orbital. We study the plot of absorbance measured in the end, to that of the input wavelength of light, to understand transitions of electrons in the molecule.

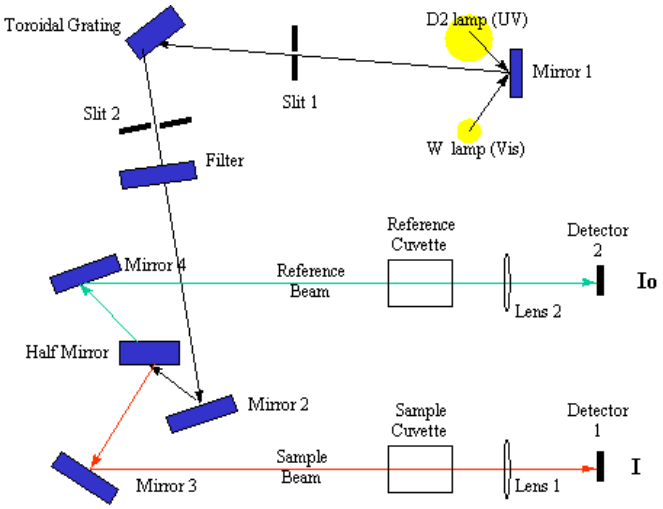

Figure 7.6: Schematic Diagram of UV-Vis Spectrometer

.

UV-Vis Spectrometer (Fig 7.6), consists of UV (or) Visible light source emitting the corresponding wave. It gets split into components of different wavelengths using prism/diffraction grating. Using a half mirror, the input light is split into two beams of same intensity. While one beam is studied as reference (Using transparent solvent/mentioned solvent), the other beam passes through the sample. Both output intensities are then measured by detectors and compared. For this research work, the sample was measured, using, Perkin Elmer Lambda 35 UV-Vis spectrometer in the range of 200-1100 nm.

Chapter 8

Z-Scan Technique

Different characterization techniques can be used to measure third-order nonlinearities, including third harmonic generation, optical Kerr effect, degenerate four wave mixing, two-beam coupling, ellipse rotation, time related single photon counting, etc. There techniques are sensitive and helpful, but quite complex. The idea of z-scan technique was first given by Sheik-Bahae et al and was found that this characterization technique was highly sensitive as well as simple to measure.It measures third-order optical nonlinearity and also helps us to find how nonlinear absorption and refraction affects the nonlinearity of the sample. Thus, this technique was preferred to evaluate nanofibers in this research work. I have gone along with open aperture z-scan for the non linear optical measurements.

8.1 Two-photon and multi-photon Absorption

Two photon Absorption explains the process of transition of the atoms/molecules of the material from ground state to a higher and excited state through a virtual intermediate state, while two photons are simultaneously absorbed (Fig 8.1). Göppert-Mayer was the first scientist to predict the two photon transition probability using second order pertubation theory in 1931. From Eq. (32), we can simplify and write as

$$\frac{dI}{dz} = -\beta I^2 \tag{33}$$

Multi photon Absorption, as the name implies, uses three or multiple (n) photons to absorb and transition from ground state to higher state, having to cross (n-1) virtual states during the process. The previous equation can be changed accordingly by replacing 'β' with 'α_n' for n photon absorption coefficient, to get

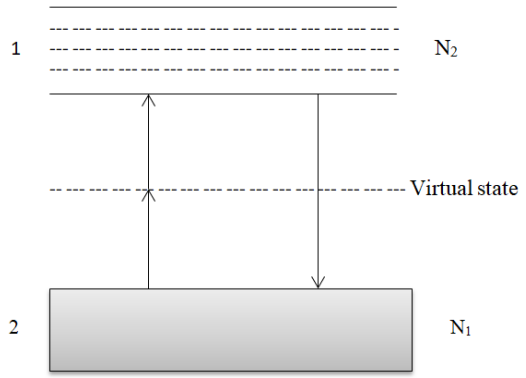

Figure 8.1: Energy level diagram of two-photon absorption

$$\frac{dI}{dz} = -\alpha_n I^n(z) \tag{34}$$

Integrating, the equation changes as

$$\int_{I_{in}}^{I_{out}} \frac{dI(z)}{I^n(z)} = -\alpha_n \int_0^L dz$$

$$\left[\frac{I^{-n+1}}{-n+1}\right]_{I_{in}}^{I_{out}} = -\alpha_n L$$

$$\frac{1}{n-1}\left[\frac{1}{I_{in}^{n-1}} - \frac{1}{I_{out}^{n-1}}\right] = \alpha_n L$$

$$\frac{1}{(n-1)I_{in}^{n-1}}\left[1 - \frac{1}{T^{n-1}}\right] = \alpha_n L$$

where transmittance $T = \frac{I_{out}}{I_{in}}$. Now

$$T = \frac{1}{\left[1 + (n-1)\alpha_n L I_{in}^{n-1}\right]^{1/(n-1)}}$$

Using $I_{in} = \frac{I_{00}}{\left[1+(z^2/z_o^2)\right]}$, we get transmittance n Photon Absorption as

$$T = \frac{1}{\left[1 + (n-1)\alpha_n L \left[\frac{I_{00}}{\left[1+(z^2/z_o^2)\right]}\right]^{n-1}\right]^{1/(n-1)}} \tag{35}$$

where n = 2,3,4..., 'I_{00}' defines peak intensity, 'I_{in}' is the intensity at sample position, 'I_{out}' is output intensity, 'Z_o' is Rayleigh range, and 'ω_o' is beam waists at focal point.

For a given nonlinear material, if absorption cross-section of the excited state is small compared to that of ground state, the transmittance of a given nonlinear material increases under strong excitation. This results in Saturable Absorption(SA) Process. If the otherwise case happens, i.e, absorption cross-section of excited state is more to that of ground state, the material gives less transmission, resulting in Reverse Saturation Process(RSA) Process.

Using high intensity pulsed lasers, the processes of two and multi photon absorption has been widely researched recently. These processes have been implemented in various nonlinear optical devices, including optical limiters[22], data storage[23], microfabrication[24], etc

8.2 Experimental Setup

There are 2 types of z-scan measurements. Closed z-scan measurements, helps in calculating nonlinear refractive index of given material. Open z-scan measurements, helps in measuring nonlinear absorption coefficient of the sample. The Schematic Experimental Setup for the open z-scan is as follows,

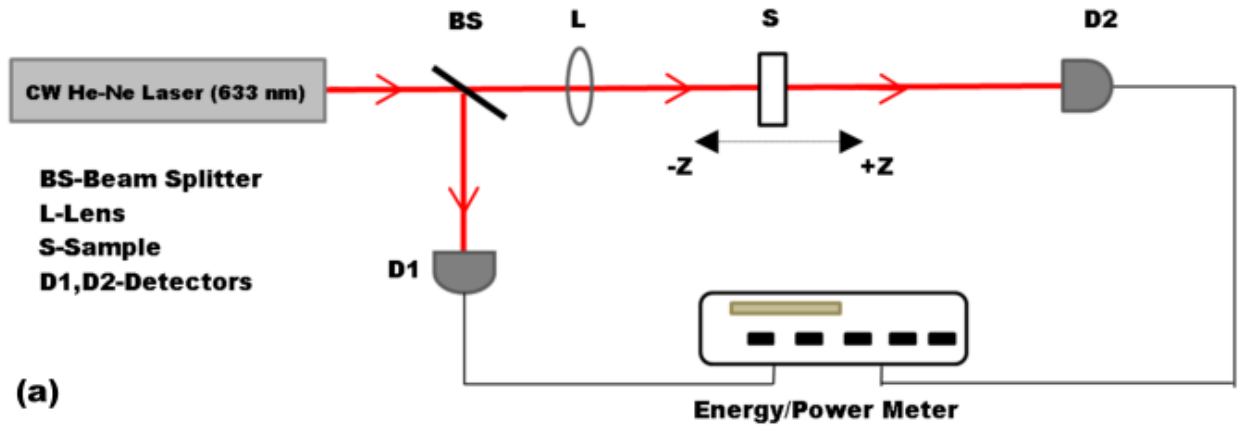

Figure 8.2: Z-scan in circuit form (For open case, there is no aperture in front of the detector).

In this experiment, the sample is traversed from one end, through the focus(z=0), to the other end, along z direction, when highly intense Gaussian beam is shone upon the sample, also propagating along z axis. As the sample moves, transmittance is measured by the detector, for every point in z direction, and the graph is plotted between normalized transmittance and Z axis (Fig 8.2).

The difference between open and close z-scan measurements is that, there exists another aperture in be-

tween the sample and the detector. This can be moved along so that the results can be used to calculate nonlinear refractive index, whereas open z-scan is impertinent to NRI.

Since there is no aperture, The resultant graphs obtained from open z-scan has to be symmetric with a valley or a peak at the focus(z=0) (Fig 8.3). When the transmittance forms a peak, then it is SA Process, whereas if the transmittance forms a valley, then, it is RSA Process.

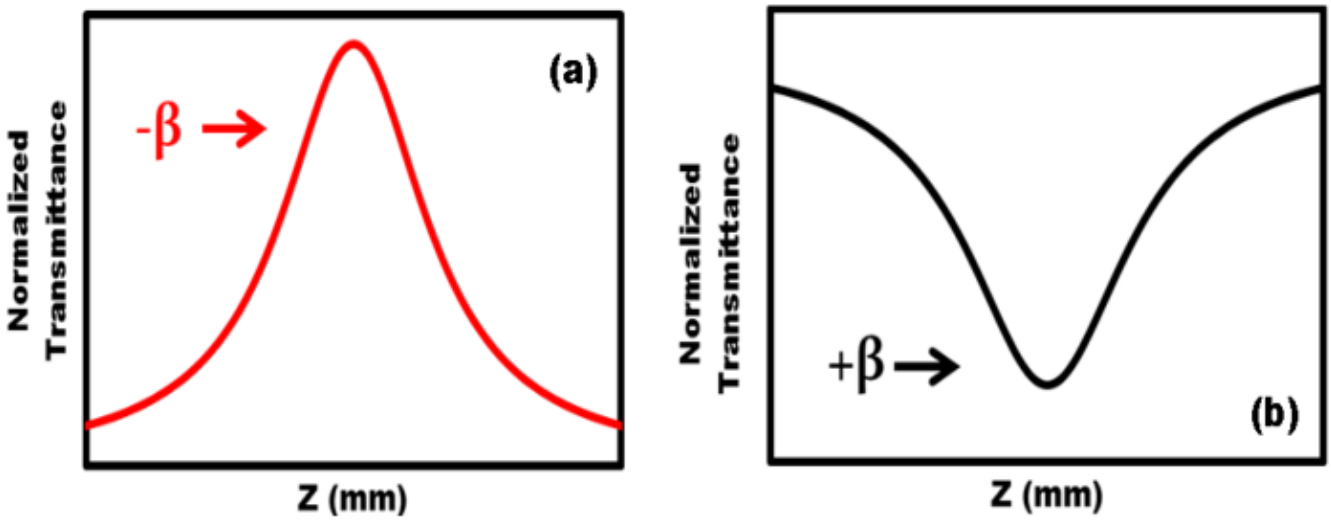

Figure 8.3: Open aperture z-scan curves(a) Saturable Absorption and (b)Reverse Saturable Absorption.

8.3 Theory

Nonlinear Susceptibility of the third- order can be split into real and imaginary parts$\chi^{(3)} = \chi^{(3)}_{Real} + i\chi^{(3)}_{Imag}$, where,

$$\chi^{(3)}_{Real} = 2\eta_o^2 \varepsilon_o c\gamma \tag{36}$$

, and

$$\chi^{(3)}_{Imag} = \frac{n_o^2 \varepsilon_o c\lambda\beta}{2\pi} \tag{37}$$

Here, nonlinear refractive indices, 'n_2'(in esu) and 'γ'(in m^2/W) is related by $n_2 = \frac{cn_o}{40\pi}\gamma$. Since the laser is set in for second harmonics, the process can be considered as a two- photon absorption process, from Eq (32), we can simplify it to get $\frac{dI}{dz'} = -\alpha(I)I, where \alpha(I) = \alpha + \beta I$.

We can calculate irradiance distribution, $I_e(z,r,t) = \frac{I(z,r,t)e^{-\alpha L}}{1+q(z,r,t)}$, and phase shift of the laser at exit surface, and can be coupled, to give Complex Electric field at the exit surface, as,

$$E_e = E(z,r,t)e^{-\alpha L/2}(1+q)^{(ik\gamma)/(\beta-1/2)} \tag{38}$$

where 'L' is defined as interaction length of the sample, $q = \beta I(z,r,t)L_{eff}$ and effective length, $L_{eff} = (1-e^{-\alpha L})/\alpha$

Transmitted power can be calculated, by integrating Irradiance distribution, at z over r(refer [25,26] for detailed derivation),

$$P(z,t) = P_i(t)e^{-\alpha L}\frac{ln[1+q_0(z,t)]}{q_0 t} \tag{39}$$

where $q_0(z,t) = (\beta I_{00}(t)L_{eff})/(1+z^2/z_o^2)$. Time integration of previous equation, can give normalized Transmittance(assuming S = 1, for open case),

$$T(z,S=1) = \frac{1}{\sqrt{\pi}q_0(z,0)}\int ln\left[1+q_0(z,0)e^{-\tau^2}\right]d\tau \tag{40}$$

.

For $|q_0| < 1$, the above equation can be expressed in terms of peak irradiance as,

$$T(z,S=1) = \sum_{m=0}^{\infty}\frac{[-q_0(z,0)]^m}{[m+1]^{3/2}} \tag{41}$$

.

The equation (41) is used to calculate nonlinear absorption coefficient 'β' in the open z-scan measurements.

Finally, Simplifying the output power in Eq (39), we can get the output fluence F(z), as,

$$F(z) = \frac{4\sqrt{ln2}E_{in}}{(\pi^{3/2}\omega^{(2)}(z))} \tag{42}$$

From the previous equation (40), it is easy to prove, that at sufficient high intensities/fluence, the material deviates from normalized transmittance of 1, and either increases or decreases. The rate of increase/decrease depends on the NLO absorption properties of the media.

8.4 Advantages and limitations

Advantages of z-scan, include

- Simplicity and Sensitivity are high compared to other techniques, in calculating nonlinear absorption coefficients and refractive index.
- Setting up of the Instruments required for the basic setup is easy, as the person only has to work on the alignments, and elevation.
- For the open case, It can determine imaginary part of third nonlinear susceptibility, whereas along with closed z-scan, It is easy to determine both real and imaginary parts.
- The technique can be used to study nonlinear refractive index, and is easy to find the sign and magnitude of NRI
- Data Analysis for the basic versions are uncomplicated, quick, and easy to understand.
- A slight Alteration in the experiment, can allow us to study nonlinearities of higher order.

Limitations of z-scan, come from

- Measurements can be accurate, only if the incoming beam is high quality Gaussian TEM_{00} beam.
- If non Gaussian beam is in case used, The data analysis can be a little laborious and difficult.
- If the experiment is changed so that a second beam is needed, the alignments and elevations play a major role in analysis and the final result of the experiment.
- Simple and ordinary mistakes, like Sliding of sample from the moving mount during the experiment, Sample distortions, can distract the beam, off the far field aperture.

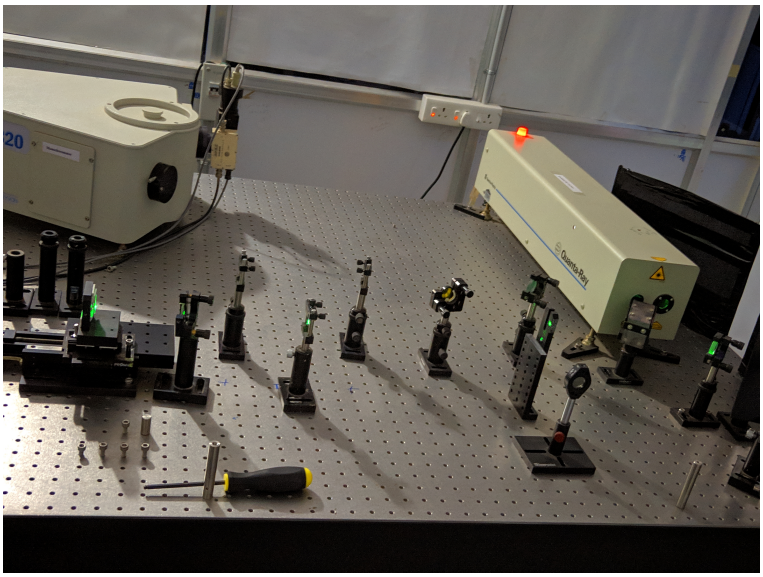

Figure 8.4: Z scan Measurements

Open aperture Z-scan measurements was done using Nd:YAG laser of wavelength λ 532 nm with pulses coming at a width 'p_t' 5 ns. This is done by creating second harmonics of laser(wavelength 1064 nm) and by Q switching, to get laser bursts. The optical table is mounted with lens of focal length 10 cm and the incident energy 'E' of the laser beam is kept constant around 100μ J(Using Half lens to cut 50% intensity of incident beam), and fibers of 2:1 and 1:1 ratio is studied for third- order nonlinear absorption.

Part III

Results and Conclusions

Chapter 9

Results and Discussion

Initial stages of material preparation was tumultuous, since one has to test different ratios and parameters, before one can conclude with a successful nanofiber layer bed. PVA Weight percent with respect to water, had to be close to 13% for the nanofiber to form along with Urea, as lesser concentrations led to charged droplet spray, and higher weight percents led to blockage of the solution at the tip. This result matches with the literature[27]. For the nanofiber to form with Urea embedding inside the matrix, or to form inclusion complex, Maximum weight ratio accepted was 1:1. Lower than 2:1 did not even result in formation of nanofibers. This could be hypothesized that as concentration of urea decreases, PVA acts more like the case of just the polymer being used, resulting in blockage of the tip(as the weight percent of PVA only case for electrospinning is less than 10%[28]). The Voltage and Flow rate of 19kV and 0.2ml was chosen as more than the above values, result in spraying, and lesser values confine the formations of fibers. Distances less than 17cms from collector to syringe, results in smudging of the solution at the drum.

9.1 SEM Analysis

The structure, morphology and size of PVA:Urea Fibers of different ratios were analysed using Scanning Electron Microscopy (Fig 9.1). From six different SEM images, obtained for the three different samples under two different magnifications, the optimal electrospun fibers of 1:1 ratio, seems to be cylindrical and homogeneous, with its diameter in the range of nanometers.This SEM result matches with the literature[10]. But it is easy to see that as Urea concentration decreases, beaded morphologies increases.

Beaded morphologies attribute to more viscocity and surface tension of the solution. Hence we can say that as concentration of Urea decreases, PVA monopolized the fiber, confirming our previous guesses. Even

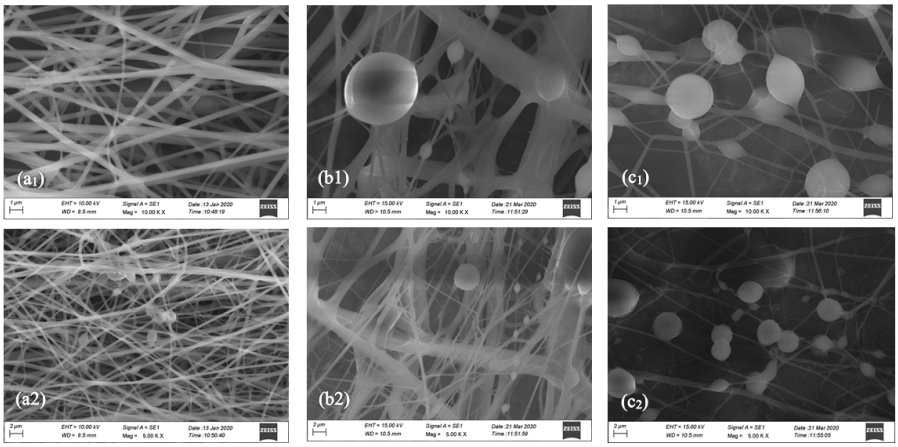

Figure 9.1: SEM Images of PVA-Urea fibers, in (a) 1:1 ratio, (b) 4:3 ratio, and (c) 2:1 ratio, with different magnification.

though I expected aligned fibers in the sample, this was not the case. One can easily refer from Fig 6.1 , that the jet evolves into a web like structure at the other end, which implies to nonaligned, mesh like fiber layer.

Since both the lower concentrations have beaded morphologies, and SEM image of 4:3 ratio looks damaged and smudged, we hereafter, use fiber of ratio 1:1 for remaining characteristic studies and add fiber of ratio 2:1 for comparative studies of linear and nonlinear absorption.

9.2 X-Ray Diffraction Analysis

The XRD Pattern was obtained for PVA-Urea fiber of ratio 1:1, to find crystal structure and orientations of the Urea molecule, in the layer bed.

Results from the plot 9.2 show that there is a very large single peak at $2\theta = 22.28^o$. From Bragg's law, $n\lambda = 2dsin(\theta)$, we can find 'd', since wavelength of incoming beam is mentioned before as 1.5406$\AA$ and 'n' can be considered to be one. The value of 'd' is calculated to be 3.988 $\AA$.

From Urea reference card, we know that it has tetragonal crystal lattice, where the peak matches with crystal plane of (110). Using the miller equation for tetragonal symmetry, $\frac{1}{d^2} = \frac{h^2+k^2}{a^2} + \frac{l^2}{c^2}$ and a:c ratio of Urea, we can get all the unit cell parameters (Table 9.1).

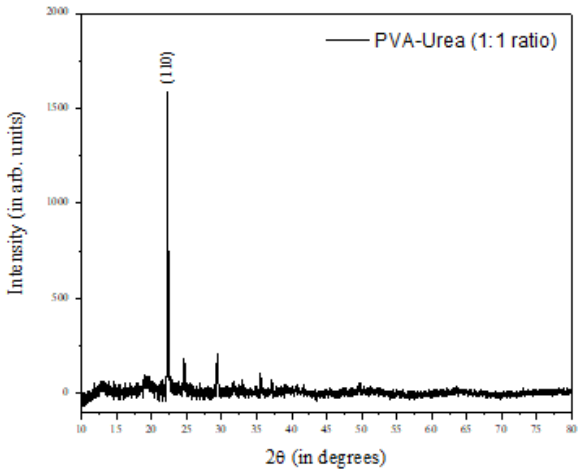

Figure 9.2: X-Ray Diffraction Image for PVA-Urea Fiber of ratio 1:1

SI. No	**Structural details**	
1	Empirical Formula	CH_4N_2O
2	Crystal System	Tetragonal-Scalenohedral
3	Space Group	$P\bar{4}2_1m$
4	$\alpha = \beta = \gamma$	90^o
5	Color	White
Unit Cell Dimensions Comparison		
	Literature	**Experiment(with average errors)**
a	5.646Å	$5.641 \pm (2.139x10^{-4})$Å
b	5.646Å	$5.641 \pm (2.139x10^{-4})$Å
c	4.701Å	$4.697 \pm (1.782x10^{-4})$Å
V	$149.86Å^3$	$149.44 \pm (1.70x10^{-2})Å^3$

Table 9.1: Structural Details of Urea

Using Scherrer formula for an idealistic value of 'K' = 0.9 and Full Width at Half Maxima measured to be 0.1482^o, we get crystalline size 'D' of the spherical crystal around 54.635 nm. The results from calculations and table 9.1 show that, Urea lies embedded inside the PVA fiber matrix mostly in (110) plane, and its polarizable axis, parallel to the polymer fiber.Therefore, it can be considered as pseudo- one dimensional crystalline structure as same as that of urea in single crystal bulk. This verifies with the literature work done already[10]. The Unit cell parameters also match with the bulk, with slight errors.

9.3 FTIR Spectroscopy

Using FTIR Spectroscopy, Functional groups of PVA and Urea, reacting with respect to its vibrational frequencies have been studied. The fiber was measured in the range of $4000 - 400 cm^{-1}$. The observed peaks, its corresponding molecular vibrations can be seen in the Spectroscopy graph (Fig 9.3),

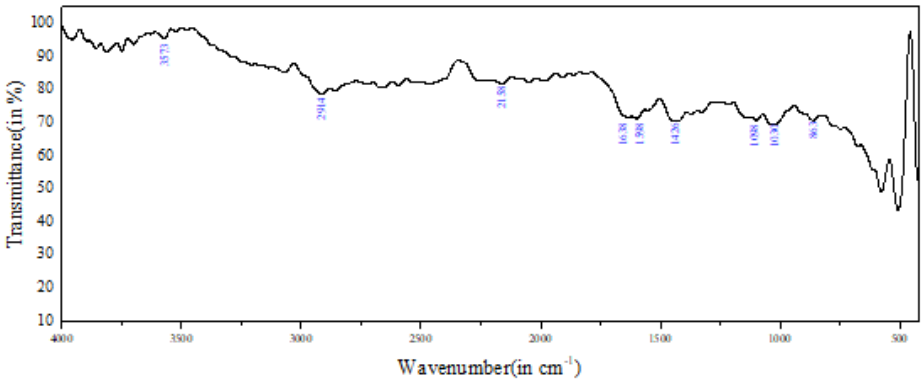

Figure 9.3: FTIR Spectroscopy for PVA-Urea Fiber of ratio (1:1)

S. No	Wavenumber (in cm^{-1})	Assignments
1	3573.65	O-H Stretching
2	2913.51	CH_2 Symmetric Stretching
3	1638.29	N-H Bending
4	1598.52	$C = O$ and NH_2 Bending
5	1426.37	C-H bending in CH_2
6	1098.73	C=O Stretching
7	1030.73	C-N Stretching
8	862.93	C-C Stretching

Table 9.2: FTIR Peaks and corresponding bands in PVA and Urea

From the previous graph results and comparing with literature [29,30], we can see different vibrational modes of molecules(Table 9.2). Wavenumbers (in cm^{-1}) 3573.65, 2913.51, 1098.73, 1030.73 and 862.93, corresponds to stretching of O-H, CH_2, C=O, C-N, and C-C molecules. whereas, NH_2, N-H and C-H bending corresponding wavenumbers of 1598.52, 1638.29, and 1426.37 $cm^{-1}s$. The Wavenumber of 2158.47 cm^{-1} not mentioned in the table, corresponds to C-C Weak streching and C-H Rocking. It can be seen that the

peaks from the spectrometer are not sharp enough and some of them was broad. Either there were no change in dipole moment on the molecule(which is unlikely), or the outgoing photons gets too much scattered, making them fall less onto the detectors.

9.4 Ultra Violet-Visible Spectroscopy

Linear Absorption for the fibers is studied using this characterization technique, where, the input range was specified as 200-1100 nm.

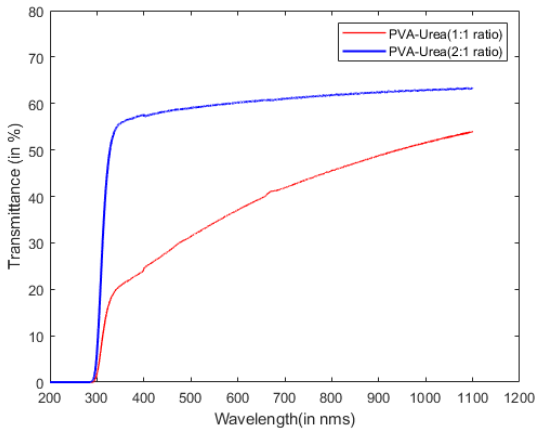

Figure 9.4: UV Spectroscopy for PVA-Urea fibers of ratio 4:3, and 1:1

From the above plot (Fig 9.4), we can conclude that, as Urea concentration increases, Intensity of absorbance increases, which results in decrease in transmittance, We can also see that around 300 nm(Cutoff Wavelength), The transmittance rises sharply(due to the presence of Urea), and the fiber of lowest concentration, hits optical transmittance of around 65 %.

9.5 z-scan measurements

The open aperture Z-scan technique was used to measure nonlinear absorption of two fibers of different concentration ratios. As mentioned previously, Pulsed Nd:YAG laser ($\lambda_o = 1064nm, p_t = 5ns$) undergoes Second Harmonic Generation($\lambda = 532nm$). It is then concentrated using diffraction slits and lens (f = 10cm), and input intensity is reduced to 100 μJ.

Beam waist 'w_o' is calculated around 9.412μm. Then the Rayleigh range 'Z_{oo}' is calculated using the formula, $Z_{oo} = \pi w_o^2/\lambda$. This value comes around 0.555 mm. The incident intensity can be found using

the formula $I_o = \frac{\pi E D^2}{4\lambda^2 L^2 p_t}$, where 'D' is the diameter of Laser falling onto the lens and 'L' being the sample thickness of the Laser(measured to be 0.18 mm). Using this formula and the observations from the previous equations, we get $I_o = 2.465x10^{12} W/cm^2$.

The Equation (35) is used for calculating nonlinear absorption coefficients of the fibers. In this case, only third order is considered, hence n = 2. The nonlinear curve is varied so that, it matches approximately with the measured points, and its corresponding 'β' values are noted.

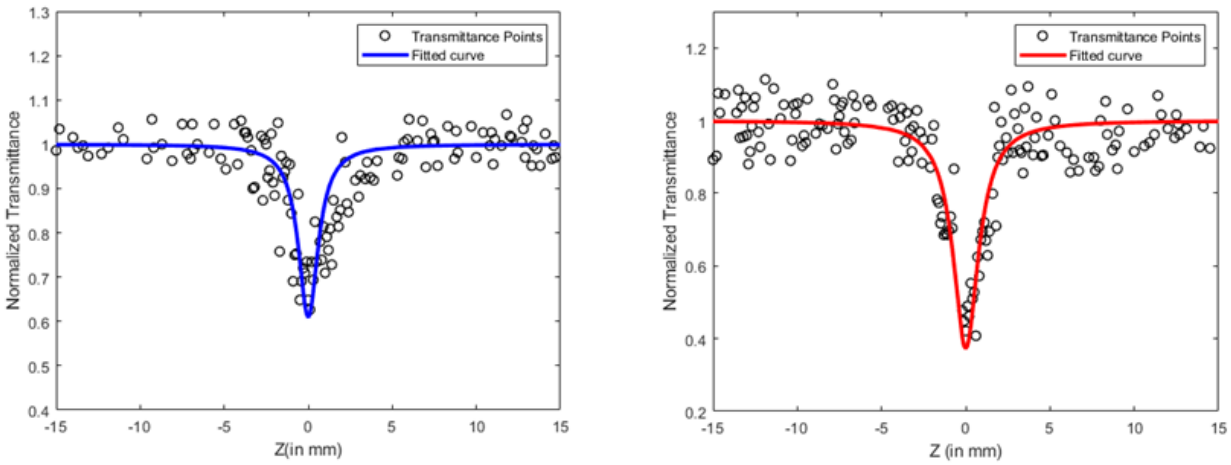

Figure 9.5: Open aperture Z-Scan Measurements of (a) 2:1 PVA Urea fiber, (b) 1:1 PVA Urea fiber

From the data measured from the open z- scan technique, we can say that the fibers exhibit Reverse Saturation Process, the case in which the observed material, absorbs more of the laser, due to high value of nonlinear absorption coefficient'β'. It is also easy to compare the two graphs, and can be concluded, that as concentration increases,normalized transmittance decreases, which implies there is an increase in the value of 'β'.

The curve fit was done using nonlinear regression methods in Matlab and the points which were heavily deviating from the curve fit, was removed using Origin software (Fig 9.5). The 'β' values of the curves were approximately $1.448x10^{-13}$m/W for the fiber of 2:1 ratio, and $3.7933x10^{-13}$m/W for the fiber of 1:1 ratio. From the above graphs, we can see that 'β' values increases, as concentration of urea increases in the electrospun fiber. Since the sample is made of fibers, there is a high possibility of scattering in the laser output, and the sensitive detector, can measure multiple scattered points in a single cross sectional area, and the average, may not match with the curve fit. Hence we can see that there are many other points which does not fit with the equation curve.

Chapter 10

Conclusions

Nanofibers of PVA(Polyvinyl Alcohol)-Urea , were prepared using electrospinning method. The electrospun fibers, when seen in SEM images, show homogeneity and cylindrical structure for ratio of 1:1, and displays beaded morphologies in others. The XRD Pattern of the fibers, show urea in its tetragonal crystal system, mirroring its one dimensional crystal nature of the bulk. The space group was confirmed to be $P\bar{4}2_1m$, and its unit cell measurements is almost as same as the urea in crystal bulk albeit small errors. The FTIR spectral plots, shows all the fundamental molecules and its vibrational spectroscopies, explaining intermolecular bonding of various degrees. The Linear absorption was studied using UV-Vis spectrometer, and the results conclude that the materal exhibits lower transition, as Urea concentration ratio, increases within the molecule. Nonlinear absorption was measured using open aperture z scans, whose results shows that urea, has the possibility to exhibit third-order nonlinear optics, by showing Reverse Saturation Process. The nonlinear absorption coefficient increases for increase in concentration of urea, and the optimal ratio gives a 'β' value of $3.7933x10^{-13}$m/W which shows its efficiency as an optical limiter device. Finally, I finish by saying that nanostructures are indispensable in our day to day devices, and these type of fibers brings us an opportunity to study and research different unique and various applications of the mentioned structures. We have just scraped out from the bottom and have to go through a lot inorder to reach the sky.

Bibliography

References

[1] Feitelson, D.G. , *Optical computing: A survey for computer scientists*, United States(1988).

[2] Andrzej Feliks Przylipiak, Elżbieta Galicka, Magdalena Donejko, Marek Niczyporuk, and Jerzy Przylipiak , *A comparative study of internal laser-assisted and conventional liposuction: a look at the influence of drugs and major surgery on laboratory postoperative values*, Drug design, development and therapy **7**, 1195-200(2013).

[3] Frank L. Pedrotti, Leno M. Pedrotti and Leno S. Pedrotti, *Introduction to Optics*, 143-146, (Addison-Wesley, 2006).

[4] J. E. Geusic, H. M. Marcos, and L. G. Van Uitert, *Laser oscillations in Nd-doped yttrium aluminum, yttrium gallium, and gadolinium garnets*, Appl Phys Lett **4**, 182(1964).

[5] A. Yariv, *Quantum Electronics*, 378-384, (John Wiley and sons, 1989).

[6] Robert W. Boyd, *Nonliear Optics, 2nd Edition*, 32-53, (Academic Press, 2003).

[7] B.E.A Saleh and M.C.Teich, *Fundamentals of photonics, 2nd Edition*, 906-915, (John Wiley and sons, 2007).

[8] J.L.Oudar and H.Le Person, *Second-Order Polarizabilities of Some Aromatic Molecules*, Optics Communications **15**, 258–262(1975).

[9] Dmitry Isakov, Etelvina de Matos Gomes, Igor Bdikin, Bernardo Almeida, Michael Belsley, Margarida Costa, Vitor Rodrigues, and Alejandro Heredia *Production of Polar β-Glycine Nanofibers with Enhanced Nonlinear Optical and Piezoelectric Properties*, ACS Crystal Growth and Design**11(10)**, 4288-4291(2011).

[10] D. Isakov , E. de Matos Gomes, M. Belsley, B. Almeida, A. Martins, N. Neves and R. Reis, *High nonlinear optical anisotropy of urea nanofibers*, Europhysics Letters **91**, 2(2010)

[11] E. Delahaye, N. Sandeau, Y. Tao, S. Brasselet and R. Clement,*Synthesis and Second Harmonic Generation Microscopy of Nonlinear Optical Efficient Hybrid Nanoparticles Embedded in Polymer Films. Evidence*

for Intra- and Internanoparticles Orientational Synergy, The Journal of Physical Chemistry C **113(21)**, 9092-9100(2009).

[12] D. Brasselet and J. Zyss, *Nonlinear polarimetry of molecular crystals down to the nanoscale*, J. physique **8**, 165(2007).

[13] Dmitry V. Isakov, Etelvina de Matos Gomes, Luis G. Vieira, Tatsiana Dekola, Michael S. Belsley, and Bernardo G. Almeida, *Oriented Single-Crystal-like Molecular Arrangement of Optically Nonlinear 2-Methyl-4-nitroaniline in Electrospun Nanofibers*, ACS Nano **1**, 73(2011).

[14] H. Tadokoro.; T. Yoshihara, Y. Chatani and S. Murahashi, textitA preliminary report of structural studies on polyethylene oxide-urea complex, Journal of Polymer Science B **2(4)**, 363–368(1964).

[15] Seema Sharma, *Ferrolectric nanofibers: principle, processing and applications*, Advanced Materials Letters **4(7)**, 522-533(2012).

[16] D. Li and Y. Xia, *Electrospinning of Nanofibers: Reinventing the Wheel?*, Advanced Materials**16(4)**, 1151-1170(2004).

[17] W. Zhou, R. Apkarian, Z.L Wang and D. Joy, *Fundamentals of Scanning Electron Microscopy (SEM)*, Scanning Microscopy for Nanotechnology, 2–7(2006).

[18] L Reimer, *Scanning Electron Microscopy: Physics of Image Formation and Microanalysis, 2nd edition*, 2, (Springer, 2013).

[19] M. Eckert, *Max von Laue and the discovery of X-ray diffraction in 1912*, Ann. Phys. **524(5)**, A83-A85(2012).

[20] Y. Waseda, E. Matsubara and K. Shinoda, *X-Ray Diffraction Crystallography- Introduction, Examples and Solved Problems*, 123-127 ,(Springer, 2011).

[21] H. Spinrad and R.F. Wing, *Infrared Spectra of Stars*, Annual Review of Astronomy and Astrophysics **7**, 249(1969).

[22] Eric W. Van Stryland, H. Vanherzeele, M. A. Woodall, M. J. Soileau, Arthur L. Smirl, Shekhar Guha and Thomas F. Boggess, *Two Photon Absorption, Nonlinear Refraction, And Optical Limiting In Semiconductors*, Optical Engineering **24(4)**, (1985).

[23] James H. Strickler and Watt W. Webb, textitThree-dimensional optical data storage in refractive media by two-photon point excitation, Optical Letters **16(22)**, 1780-1782(1991).

[24] Shoji Maruo, Osamu Nakamura, and Satoshi Kawata, *Three-dimensional microfabrication with two-photon-absorbed photopolymerization*, Optical Letters **22(2)**, 132-134(1997).

[25] M Sheik-Bahae, A.A Said and E.W Van Stryland, *High-sensitivity, single-beam N2 measurements*,

Optics letters **14(17)**, 955-957(1989).

[26] M Sheik-Bahae, A. A Said, T. H Wei, D.J Hagan and E.W Van Stryland, *Sensitive measurement of optical nonlinearities using a single beam*, IEEE Journal of Quantum Electronics **26(4)**, 760-769(1990).

[27] I. Hassounah, N. Shehata, A. Hudson, B. Orler and K. Meehan, *Characteristics and 3D Formation of PVA and PEO Electrospun Nanofibers with Embedded Urea*, Journal of Applied Polymer Science, **131(3)**, (2013).

[28] Jong-Chul Park, Takeru Ito, Kyu-Oh Kim, Kwan-Woo Kim, Byoung-Suhk Kim, Myung-Seob Khil, Hak-Yong Kim and Ick-Soo Kim, *Electrospun poly(vinyl alcohol) nanofibers: effects of degree of hydrolysis and enhanced water stability*, Polymer Journal **42**, 273–276(2010).

[29] I. Omkarama, R.P. Sreekanth Chakradhar and J. Lakshmana Rao, *EPR, optical, infrared and Raman studies of* VO^{2+} *ions in polyvinylalcohol films*, Physica B:Condensed Matter **388(1-2)**, 318-325(2007)

[30] Z. Piasek and T. Urbanski, *The Infra-red Absorption Spectrum and Structure of Urea*, B Pol Acad Sci-Tech **10(3)**, (1962).